J Mater Sci (2010) 45:4659–4664
DOI 10.1007/s10853-010-4604-3

ULTRAFINE GRAINED MATERIALS

Grain refinement in nanostructured Al–Mg alloys subjected to high pressure torsion

Manping Liu · Hans J. Roven · Xintao Liu · Maxim Murashkin · Ruslan Z. Valiev · Tamas Ungár · Levente Balogh

Received: 12 February 2010 / Accepted: 6 May 2010 / Published online: 18 May 2010

Abstract Nanostructures of three binary Al–Mg alloys and a commercial AA5182 alloy subjected to high pressure torsion at room temperature were comparatively investigated using transmission electron microscopy, high-resolution transmission electron microscopy, and X-ray line profile analysis. Grain size distributions, dislocation densities, and densities of planar defects including stacking faults and microtwins were quantified. The average subgrain size decreased considerably from 120 to 55 nm as the Mg content increased from 0.5 to 4.1 wt%. The average dislocation density in the alloys first increased to a maximum and then decreased as the Mg content increased and the average subgrain size decreased. The role of Mg solute on these features and the refinement mechanisms associated with the typical nanostructures and faults were interpreted.

Electronic supplementary material The online version of this article (doi:10.1007/s10853-010-4604-3) contains supplementary material, which is available to authorized users.

M. Liu (✉) · X. Liu
National Engineering Research Center of Light Alloy Net Forming and State Key Laboratory of Metal Matrix Composites, School of Materials Science and Engineering, Shanghai Jiao Tong University, 800 Dongchuan Road, Shanghai 200240, China
e-mail: manping.liu@sjtu.edu.cn

H. J. Roven (✉)
Department of Materials Science and Engineering, Norwegian University of Science and Technology (NTNU), Alfred Getz vei 2b, 7491 Trondheim, Norway
e-mail: hans.roven@material.ntnu.no

M. Murashkin · R. Z. Valiev
Institute of Physics of Advanced Materials, Ufa State Aviation Technical University, 12 K. Marx Street, Ufa 450000, Russia

T. Ungár · L. Balogh
Department of Materials Physics, Eötvös University, P.O. Box 32, Budapest 1518, Hungary

Introduction

Bulk nanostructured materials (NSM) processed by severe plastic deformation (SPD) have provided new opportunities for developing nanostructures in metals and alloys with unusual properties that are very attractive for various structural and functional applications [1–4]. It is well known that solute atoms have significant effects on microstructures subjected to SPD [2, 5, 6]. However, it is still not very obvious how the microstructure features such as grain size, dislocation structures, and grain boundaries (GBs) are related to Mg solute atom contents in NSM [5–13]. Therefore, characterization of such effects should be investigated into further detail.

In this work, different Al–Mg alloys were subjected to high pressure torsion (HPT) at room temperature. The HPT processed materials were comparatively investigated using transmission electron microscopy (TEM), high-resolution TEM (HRTEM), and X-ray line profile analysis. Grain size distributions, dislocation densities, and densities of planar defects including stacking faults (SFs) and microtwins were quantified. The role of Mg solute on these features and the refinement mechanisms associated with the typical nanostructures and faults were interpreted.

Experimental

Three binary Al–Mg alloys (with 0.5, 1.0, and 2.5 wt% Mg) and a commercial AA5182 alloy (Al–4.1Mg–0.35Mn–0.13Si–0.32Fe, by wt%) received in the as-cast and

homogenized condition were subjected to HPT to five turns with a rotation speed of 1 rpm under pressure of 6 GPa at room temperature. The deformed HPT samples had dimensions of 20 mm in diameter and 0.2 mm in thickness. Small disks with diameters of 3 mm for TEM and X-ray measurements were punched from the outer edge of these HPT samples. The calculated equivalent strain at the outer edge of the HPT samples is about 906 [2]. The structural characterization was performed by both conventional TEM and HRTEM in a JEM-2010 HRTEM operated at 200 kV. Thin TEM foils were prepared from the small disks by means of disc grinding, dimpling, and finally ion polishing with Ar^+ at an accelerating voltage of 3 kV. The X-ray measurements were carried out in a special high-resolution double crystal diffractometer operated with a rotating copper anode with fine focus. The scattered radiation was registered by flat imaging plates of a linear spatial resolution of 50 μm. The four imaging plates were placed at a distance of 500 mm from the specimen in order to achieve the required high resolution and to cover the angular range of diffraction from $2\theta = 30°$ to 140°. For further details of the principles and procedures of the X-ray evaluations, please refer to [14].

Results

The general microstructures as quantified by X-ray line profile analysis are shown in Table 1 and Fig. 1. The X-ray measurements demonstrate that the content of Mg strongly influences the subgrain size of the investigated alloys. The average subgrain size, $\langle x \rangle_{\text{area}}$, decreased considerably from about 120 to 55 nm as the Mg content increased from 0.5 to 4.1 wt%. For the Al–0.5Mg alloy, the subgrain size distribution varies from 50 to 200 nm and the average subgrain size measured from the X-ray line profile analysis was about 120 nm (Table 1; Fig. 1). By comparison, the microstructure in the AA5182 alloy exhibits a subgrain size ranging 10–130 nm and has a much smaller average size of about 55 nm. As shown in Fig. 1a and b, the size distributions in all the four alloys are not uniform and grains with different size coexist. The microstructures are characterized by a log-normal size distribution and the grain size distributions became more uniform as the Mg content increased.

Interestingly, the average stored dislocation density is not changed monotonously as the Mg content increased but the average subgrain size decreased more systematically (Table 1). In other words, the dislocation density increased significantly from 1.7×10^{14} m^{-2} (Al–0.5Mg) at the average subgrain size of 120 nm, to a maximum value of 2.3×10^{15} m^{-2} (Al–2.5Mg) at the average subgrain size of 68 nm, and then decreased from this maximum value to

Table 1 The median m and the variance σ of the log-normal subgrain size distribution, the area-averaged mean subgrain size $\langle x \rangle_{\text{area}}$, the average dislocation density ρ, the dislocation arrangement parameter M, the dislocation character q, and the weighted sum of squared residuals (WSSR)

HPT alloys	m (nm)	σ	$\langle x \rangle_{\text{area}}$ (nm)	ρ (10^{14} m^{-2})	M	q	WSSR
Al–0.5Mg	108	0.194	120	1.7	1.4	0.2	
Al–1.0Mg	66	0.36	91	10	0.75	0.62	
Al–2.5Mg	48	0.36	66	25	0.9	0.7	20.5
	52	0.34	70	20	1.0	0.6	20.18
AA5182	37	0.4	55	12.8	0.9	0.7	7.12
	34	0.43	54	7.6	1.2	0.52	7.29

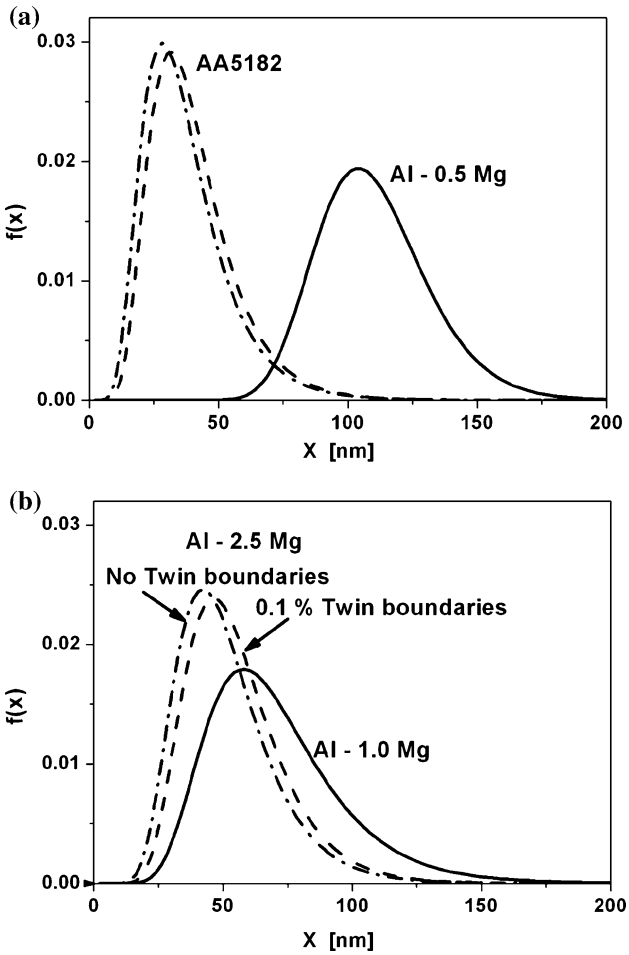

Fig. 1 Size distribution density functions assuming log-normal size distribution of subgrains: **a** Al–0.5Mg and AA5182; **b** Al–1.0Mg and Al–2.5Mg. In the case of the AA5182 alloy the two size distribution functions (*dashed* and *dash-dot line*) correspond to the two values listed in Table 1 for the two different evaluations. The difference in these two distribution functions shows the accuracy of the evaluation. In the case of the Al–2.5Mg alloy the two size distribution functions correspond to the evaluations with twins (*dashed line*) and no twins (*dash-dot line*), respectively

1.0×10^{15} m^{-2} (AA5182) at the average subgrain size of 55 nm.

Figure 2 shows the observed microstructures together with selected area diffraction (SAD) patterns taken in the TEM. The patterns exhibit diffraction rings typical for NSM, indicating random orientations in the selected field of view. Similar to the X-ray measurements, these TEM micrographs also demonstrate that the content of Mg influences strongly the mean grain size of the alloys. In addition, the TEM investigations reveal that the GB structures vary with grain size. Most grains having a size less than 100 nm have sharp GBs and are free of dislocations, i.e., no subgrains or dislocation cells were observed in these grains (see the inset in Fig. 2b). Such straight and narrow GBs are believed to be in an equilibrium state and are high angle GBs (HAGBs) [9]. In contrast, dislocation cell structures and subgrains were frequently found inside some larger grains, e.g., see the grains GB1 and GB2 in Fig. 2a. The misorientation across these cell boundaries increases with further plastic straining, and eventually becomes large enough to transform through low angle GBs (LAGBs) to HAGBs [9]. In addition, some GBs in these larger grains are often curved and poorly defined (GB2 in Fig. 2a) or have a strong spreading of thickness extinction contours (GB1 in Fig. 2a), indicating a high level of internal stresses and elastic distortions in the crystal lattice due to the presence of a high density of dislocations at the boundaries. All of these features suggest that these grains are in a non-equilibrium state and the GBs are non-equilibrium GBs.

As determined above by the X-ray line profile analysis, the average dislocation densities are in the range 1.7×10^{14} m^{-2} to 2.3×10^{15} m^{-2}. However, extensive HRTEM observations revealed that local dislocation densities in grain boundary and triple junction areas might be as high as 10^{17} m^{-2}, which are two to three orders of magnitude larger than the average values. An example of such HRTEM results is shown in Fig. 3a. This HRTEM $[1\bar{1}0]$ image is observed from a GB area in the HPT AA5182 alloy. A very high density of dislocations is found near the GB. The local dislocation density measured from this image is as high as 3.8×10^{17} m^{-2} and the corresponding average density measured by X-ray line analysis is 1.0×10^{15} m^{-2} (Table 1). The dislocations in Fig. 3a are 60° full dislocations on the $(11\bar{1})$ plane with Burgers vectors of $1/2\langle 110\rangle$. In addition, most dislocations in Fig. 3a appear as dipoles and interstitial loops and vacancy loops co-exist. Such GBs with so extreme dislocation density are non-equilibrium

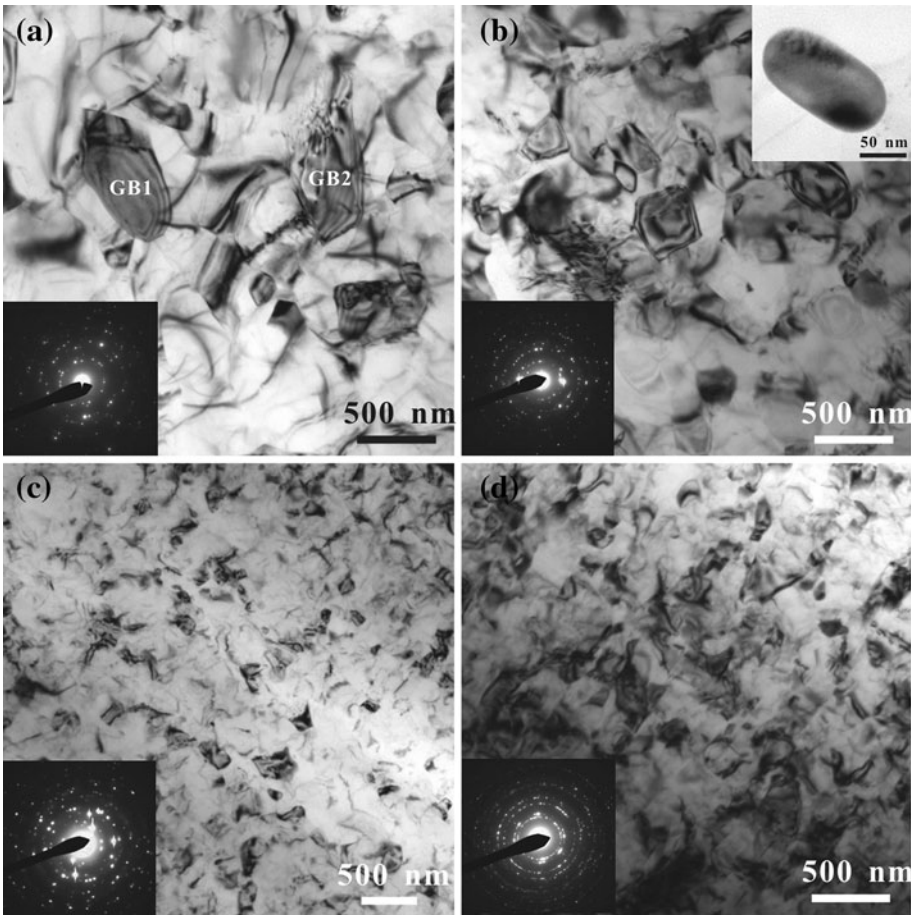

Fig. 2 TEM micrographs from the HPT Al–Mg alloys with SAD pattern insets: **a** Al–0.5Mg alloy; **b** Al–1.0Mg alloy; **c** Al–2.5Mg alloy; **d** AA5182 alloy

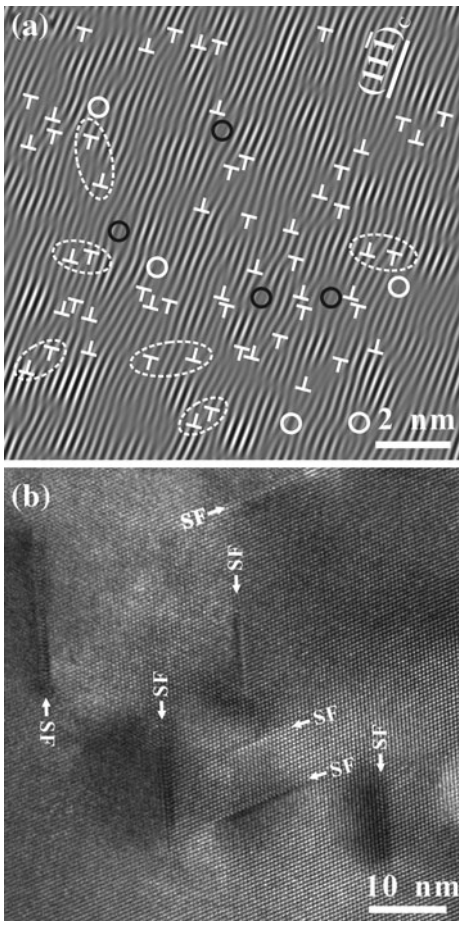

Fig. 3 HRTEM $[1\bar{1}0]$ images taken from: **a** AA5182 alloy, showing a high density of 60° full dislocations on the $(11\bar{1})$ plane near a GB area (inverse Fourier image). The ellipses show examples of dislocation dipoles. The *black circles* mark interstitial loops and the *white circles* mark vacancy loops; **b** Al–2.5Mg alloy, showing a high density of SFs (*arrows*) and microtwins within a 200 nm grain

GBs in a high energy state. Many extrinsic dislocations exist in this GB region.

Analogous to our previous works [5, 13], a high density of planar defects including SFs and microtwins was frequently detected within both nanocrystalline grains and ultrafine grains in all the four alloys. Another example of SFs and microtwins formed within ultrafine grains is shown in Fig. 3b. Several SFs can be seen inside a 200 nm grain of the Al–2.5Mg alloy. The SF widths are in the range of 5–15 nm and the local SF density is 2.0×10^{15} m^{-2}. The SFs and microtwins seemed to be preferably located in the vicinity of GBs and sub-boundaries.

Discussion

As shown in Table 1, the average dislocation density in the HPT alloys first increased to a maximum and then decreased as the Mg content increased and the average subgrain size decreased. This observation may indicate that there exist several factors that influence the dislocation density. These factors include grain size, solute effects and the HPT process parameter. All investigated samples have undergone the same deformation process but differ in their Mg contents. Thus, the change of the average dislocation density may primarily be attributed to interaction effects of solute and grain size. On the one hand, the density increases with increasing Mg solute concentration due to the increase in the Mg content. The increase in the Mg solute level leads to more trapped dislocations both in the grain interior and at GBs [10, 12]. Conversely, the average dislocation density may inversely proportional to grain size [15]. The smaller grain size makes it more difficult for dislocation pile-ups to form within grains especially when the size less than a critical value [15]. As was evident in the inset in Fig. 2b, most grains less than 100 nm are free of dislocations. Besides, the Mg solute distribution will become much more uniform as the grain size decreases to the nano-scale [7]. Consequently, the frequency of dislocation pinning by Mg solute will be weakened.

In addition to strain effects, both the X-ray measurements (Table 1; Fig. 1) and the TEM observations (Fig. 2) revealed that the Mg content plays a critical role in grain refinement. As discussed previously, the increase in the Mg level leads to more dislocations trapped by solute atoms. This indicates that more dislocations can be involved in the formation of subgrains or dislocation cell structures. In other words, the reservoir of sub-structures for fragmentation of grains is greatly increased. In addition, Mg solute atoms may also further promote the formation of dipoles and loops as shown in Fig. 3a. These defects could cause strong dislocation interactions that in turn promote structural subdivision of grains due to dynamic recrystallization under large strain [4]. Furthermore, a high density of SFs and microtwins (Fig. 3b) may also play an important role in grain refinement during SPD. Microtwins can further promote division and break-down of the grains/subgrains [16, 17]. The formation of these planar defects is also believed to be related to the combination effects of solute and strain [5, 13].

Based on the above discussions, the process of grain refinement of Al–Mg alloys during HPT can be clarified. Figure 4 is a schematic diagram showing this process. During the HPT processing with repeated turns, more and more dislocations are generated in grain interiors and at GBs due to the solute effect and large strain. As a result, dislocation cells and subgrains with LAGBs (typically in the form of non-equilibrium GBs with excess dislocations) appear within larger grains. At the same time, high-density SFs, and microtwins are formed inside grains [5, 13] and in the vicinity of GBs (Fig. 3b) resulting from dissociated

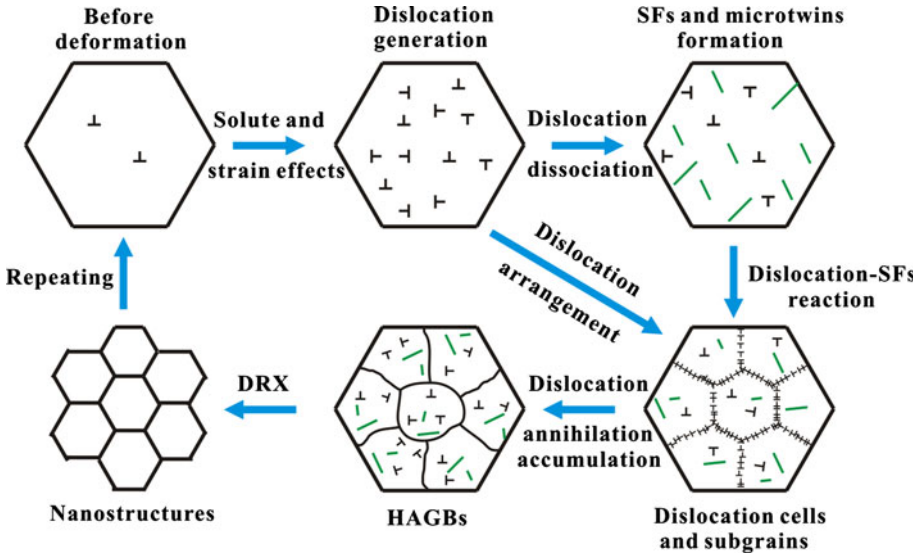

Fig. 4 Schematic illustration of the grain refinement process of Al–Mg alloys during HPT

dislocations. The formation of SFs and microtwins could also have a positive effect on the division of the grains/subgrains [16, 17]. As the dislocation density achieves some critical value with increasing strain, the misorientation across these sub-boundaries increases due to dislocation annihilation/accumulation [2, 18] and interaction of dislocations and the planar defects [2, 17]. The misorientation eventually becomes large enough to transform through LAGBs to HAGBs [9] when the density of the excess dislocations continuously rises with further plastic straining [2]. Simultaneously, the HPT process would also engage deformation heating. Once the local temperature is higher than the recrystallization temperature, dynamic recrystallization takes place. As a result, equiaxed nano-sized grains form in the regions where the highest strain is generated [18].

Summary

The average subgrain size was considerably decreased from about 120 to 55 nm as the Mg content increased from 0.5 to 4.1 wt%. The grain size distributions became more uniform as the alloying content increased. However, the average dislocation density was first increased to a maximum and then decreased as the Mg content increased and the average subgrain size decreased. This phenomenon may primarily be attributed to the interaction effects of Mg solute and grain size. The grain refinement process in these HPT alloys probably includes: (1) continuously generation of high-density dislocations resulting from the effects of solute and large strain; (2) grain division from repeated appearance of dislocation cells and subgrains with the help of the dislocation generation/reservoir; (3) formation of high-density SFs and microtwins with the dissociated dislocations; (4) gradually transformation of dislocation cells and subgrains through LAGBs into HAGBs due to dislocation annihilation/accumulation and interaction of dislocations and the planar defects; (5) finally acquisition of equiaxed nano-sized grains as a result of both the grain division and dynamic recrystallization.

Acknowledgements This work was supported by the National Natural Science Foundation of China (NSFC) under Grants No. 50971087 and the Research Council of Norway under the program SUP Light Metals Technology. One of the authors (T. U.) is grateful to the Hungarian National Science Foundation OTKA No. 67692 and No. 71594 for supporting this work. The authors also want to acknowledge the assistance of Dr. Lilya Kurmanaeva (Forschung Center of Karlsruhe, Germany), doing the tensile testing.

References

1. Valiev RZ, Zehetbauer MJ, Estrin Y, Höppel HW, Ivanisenko Y, Hahn H, Wilde G, Roven HJ, Sauvage X, Langdon TG (2007) Adv Eng Mater 9:527
2. Valiev RZ, Islamgaliev RK, Alexandrov IV (2000) Prog Mater Sci 45:103
3. Valiev R (2004) Nat Mater 3:511
4. Valiev RZ, Estrin Y, Horita Z, Langdon TG, Zehetbauer MJ, Zhu YT (2006) JOM 58:33
5. Liu MP, Roven HJ, Murashkin M, Valiev RZ (2009) Mater Sci Eng A 503:122
6. Liao XZ, Huang JY, Zhu YT, Zhou F, Lavernia EJ (2003) Philos Mag 83:3065
7. Meng QP, Rong YH, Hsu TY (2007) Mater Sci Eng A 471:22
8. Liu MP, Roven HJ, Yu YD (2008) Int J Mater Res 98:184
9. Liu MP, Roven HJ, Yu YD, Werenskiold JC (2008) Mater Sci Eng A 483–484:59
10. Chandler HD, Bee JV (1987) Acta Metall 35:2503
11. Liu MP, Roven HJ (2007) Appl Phys Lett 90:083115
12. Olmsted DL, Hector LG Jr, Curtin WA (2006) J Mech Phys Solids 54:1763

13. Liu MP, Roven HJ, Murashkin M, Valiev RZ (2008) Mater Sci Forum 579:147
14. Ungár T (2007) J Mater Sci 42:1584. doi:10.1007/s10853-006-0696-1
15. Shen TD, Schwarz RB, Feng S, Swadener JG, Huang JY, Tang M, Zhang JZ, Vogel SC, Zhao YS (2007) Acta Mater 55:5007
16. Xue Q, Liao XZ, Zhu YT, Gray GT III (2005) Mater Sci Eng A 410–411:252
17. Tao NR, Wu XL, Sui ML, Lu J, Lu K (2004) J Mater Res 19:1623
18. Ni H, Alpas AT (2003) Mater Sci Eng A 361:338